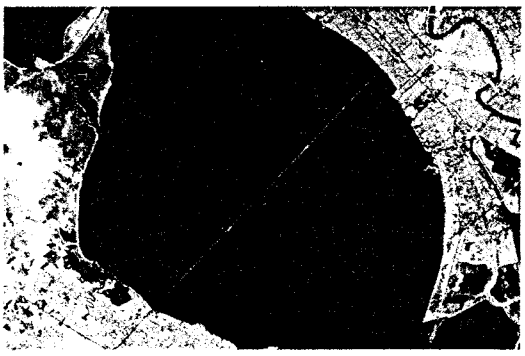

Fig. 2. Original image.

Fig. 3. Segmentation result with the proposed method.

IV. Segmentation

It is now clear that natural texture images can be discriminated by multifractal exponents. Most natural images, such as geographical images, are all textural in nature. In remote sensing images, different regions possess different texture and have different multifractal exponents. These properties are thus ideal for use in image segmentation. Like fractal dimensions, multifractal exponents are rotation invariant and intensity invariant. As these are the inherent properties of most natural regions and objects, multifractal exponents can be used to accurately describe these images.

In this simulation, four multifractal exponents ($q = -1,\ 0,\ 1,\ 2$) are chosen to segment a synthetic aperture radar (SAR) image. In order to highlight the edges, the K-means clustering approach [7], which is a fast and appropriate cluster technique for large data sets, is also applied. Using four multifractal exponents and applying the K-means method, the cluster results can be obtained. Finally, the results are mapped from the feature space to the image space.

The image we used in this paper is as shown in Fig. 2, which is a X-band SAR image spanning an area of about 100 kilometers by 50 kilometers. This is an image of the area surrounding the city of New Orleans, LA in the southeastern U.S. The image size is 520 $\times$ 450 pixels and the dark area in the center is Lake Pontchartrain. The thin line running across the lake is a causeway connecting New Orleans to the city of Mandeville.

Segmentation of the image is performed on workstation running at 250 MHz. Four multifractal exponents are estimated for each pixel based on a 15 $\times$ 15 image window. By using the K-means method, each pixel is classified into two groups: land or lake. The result obtained using the proposed method is shown in Fig. 3 in which the boundaries of Lake Pontchartrain are shown clearly and correctly, even the causeway. As multifractal exponents reflect the spatial statistics of regions/objects, they can provide a good description of the geographical image and lead to good segmentation results.

V. Conclusion

In this paper, we present a novel multifractal estimation method to describe the local scaling properties of a region/object. Computer experiments show that the proposed method performs well at different window sizes and different gray-scale levels. The proposed method has also been shown to apply successfully to the segmentation of geographical images.

References

[1] B. R. Kerman, "Information states in radar imagery of sea ice," *IEEE Trans. Geosci. Remote Sensing*, vol. 37, pp. 1435–1446, May 1999.
[2] F. P. Agterbera, Q. Cheng, A. Brown, and D. Good, "Multifractal modeling of fractures in the lac du bonnet batholith Manitoba," *Comput. Geosci.*, vol. 22, pp. 497–507, 1996.
[3] T. Falco, F. Francis, S. Lovejoy, D. Schertzer, B. Kerman, and M. Drinkwater, "Universal multifractal scaling of synthetic aperture radar images of sea-ice," *IEEE Trans. Geosci. Remote Sensing*, vol. 34, pp. 906–914, Apr. 1996.
[4] B. B. Chaudhuri and N. Sarkar, "Texture segmentation using fractal dimension," *IEEE Trans. Pattern Anal. Machine Intell.*, vol. 17, pp. 72–76, Jan. 1995.
[5] X. C. Jin, S. H. Ong, and Jayasooriah, "A practical method for estimating fractal dimension," *Pattern Recognit. Lett.*, vol. 16, no. 5, pp. 457–464, 1995.
[6] Q. Cheng, "The gliding box method for multifractal modeling," *Comput. Geosci.*, vol. 25, pp. 1073–1079, 1999.
[7] M. R. Anderberg, *Cluster Analysis for Applications*. New York: Academic, 1973.

The Multiple Interaction Model for Nonshallow Scatterers Buried Beneath 2-D Random Rough Surfaces

Magda El-Shenawee

***Abstract*—The multiple interaction model is hybridized with the robust Steepest Descent Fast Multipole Method (SDFMM) to compute the signature of nonshallow penetrable scatterers buried beneath two-dimensional random rough surfaces. The most attractive feature of the multiple interaction model with using the SDFMM is removing the quasi-planar structure constraint for analyzing nonquasi-planar scatterers. The results show that the buried object's signature is largely due to the first interaction mechanism; however, the contribution of each additional interaction is explicitly calculated, though they may become insignificant especially for lossy background soil.**

***Index Terms*—Buried objects, rough surface scattering, subsurface scattering, subsurface sensing.**

I. Introduction

Modeling electromagnetic scattering from realistic three-dimensional subsurface sensing applications requires huge number of

Manuscript received September 19, 2001; revised November 26, 2001. This work was supported by the Northeastern University ARO-MURI Grant DAA 0-55-97-0013.

The author is with the Department of Electrical Engineering, University of Arkansas, Fayetteville, AR 72701 USA (e-mail: magda@uark.edu).

Publisher Item Identifier S 0196-2892(02)04624-7.

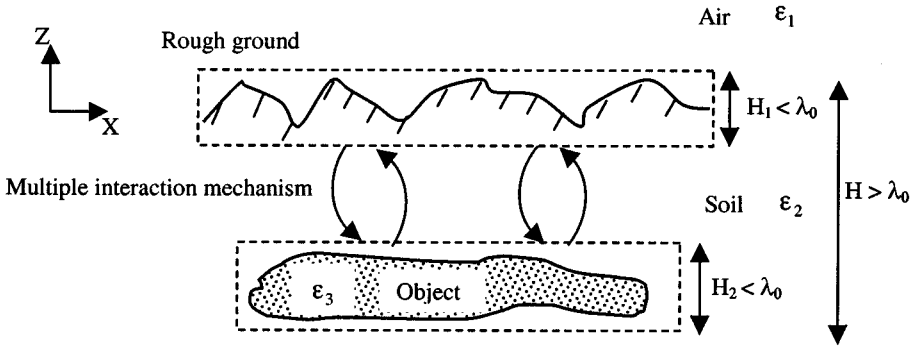

Fig. 1. Nonquasi-planar structure decomposition into two quasi-planar structures showing their multiple interactions.

computational operations that necessitates the use of fast algorithms [1]–[6]. Recently, the Steepest Descent Fast Multipole Method (SDFMM) [3] has been adopted to analyze the scattering from penetrable shallow objects buried beneath two-dimensional (2-D) random rough ground [7], [8]. The SDFMM has the great advantage of $O(K)$ computational complexity for both the CPU time and computer memory [3] compared with the $O(K^2)$ for the Method of Moments (MoM), where K is the total number of electric and magnetic surface current unknowns. However, there is a barrier that limits using the SDFMM in some applications; the whole scatterer should have a quasi-planar structure with total height equal to a fraction of a free-space wavelength. On the other hand, there are several potential applications that have nonquasi-planar geometries; e.g., the multilayered rough ground where the burial depth of the underground layer is larger than the wavelength.

The multiple interaction approach was previously used in investigating electromagnetic scattering problems either analytically from rough surfaces only (no buried objects), e.g., [9] and [10], or computationally from rough surfaces with buried objects, e.g., [11], [12]–[14]. In [9] and [10], each scattering element on the rough surface was assumed to be a second source for all scattering elements either on the same surface leading to the double scattering mechanism [9], or on the underground rough layer as presented in [10]. On the other hand, in [11], a PEC sphere was buried beneath the rough ground while in [12] and [13] a penetrable object was buried under or located above the rough ground. In addition, the multiple interaction approach is used with the Multilevel Fast Multipole Algorithm (MLFMA) for multiple targets located above the half space is presented in [14]. In these models, the coupling between the rough ground and the object is expressed as interaction matrices.

The multiple interaction approach with using the SDFMM is presented in this work. The basic idea is to decompose the three-dimensional (3-D) nonquasi-planar structure (e.g., the rough ground with a buried scatterer) into two quasi-planar scatterers as shown in Fig. 1 where the SDFMM can be used separately for each scatterer. However, the interactions between the ground and the buried scatterer are not expressed in matrices (or submatrices) but are calculated concurrently using precomputed and prestored information that facilitated the numerical evaluating of the near-field expressions given in [15]. In general, using the multiple interaction approach (with and/or without the SDFMM) enables investigating the contribution of each individual interaction mechanism between the ground and the buried object. This will greatly help in understanding the physics involved in subsurface sensing applications. It is necessary to distinguish between the multiple interaction model upon using the SDFMM, presented in this work, and our previous complete SDFMM model, presented in [7] and [8]. All the self and mutual interactions between the rough ground and the buried object were expressed as submatrices in the total impedance matrix of the whole scatterer in [7] and [8].

II. Formulation

The four integral equations describing the unknown equivalent electric and magnetic surface currents for the problem of a single object buried beneath two-dimensional rough ground were derived and discussed in [7] and [8]. The surfaces of the ground and the buried object were discretized using the RWG triangular patches [16]; and the set of linear system of equations was obtained [7], [8]

$$\begin{pmatrix} \overline{Z}_{\mathrm{g.g}} & \overline{Z}_{\mathrm{g.obj}} \\ \overline{Z}_{\mathrm{obj.g}} & \overline{Z}_{\mathrm{obj.obj}} \end{pmatrix} \begin{pmatrix} \overline{I}_g \\ \overline{I}_{\mathrm{obj}} \end{pmatrix} = \begin{pmatrix} \overline{V}_g \\ 0 \end{pmatrix} \tag{1}$$

where $\overline{Z}_{g.g}$ represents the interactions between elements only on the ground surface, $\overline{Z}_{g.obj}$ represents interactions between elements on the ground surface and elements on the object surface, $\overline{Z}_{obj.g}$ represents interactions between elements on the object surface and elements on the ground surface, and $\overline{Z}_{obj.obj}$ represents interactions between elements only on the object surface. As discussed in [7], the total impedance matrix $\overline{\overline{Z}}$ has the order of $2(N+P) \times 2(N+P)$, where N is the number of vector basis functions on the ground and P is the number of vector basis functions on the buried object. The factor of two accounts for both the electric and magnetic surface currents. The vector $\overline{V}_g$ represents the tested tangential incident electric and magnetic fields on the ground surface. The unknown coefficients $\overline{I}_g$ and $\overline{I}_{obj}$ were solved for in [7] and [8] by completely applying the SDFMM to (1), leading to converting the dense matrix $\overline{\overline{Z}}$ into a sparse one. Conversely, in this work, the multiple interaction approach will be used to solve two separate linear systems of equations for the unknown current coefficients and then iteratively update the incident fields on both the ground and the buried object as

$$\overline{Z}_{\mathrm{g.g}} \overline{I}_g^{(n)} = \overline{V}_g^{(n)} \tag{2a}$$

$$\overline{Z}_{\mathrm{obj.obj}} \overline{I}_{\mathrm{obj}}^{(n)} = \overline{V}_{\mathrm{obj}}^{(n)} \tag{2b}$$

where $n = 1, 2, 3, \ldots$ is the number of the interactions between the ground and the buried object as depicted in Fig. 2. The algorithm begins with solving (2a) for $I_g^{(0)}$, updating $\overline{V}_{\mathrm{obj}}^{(1)}$ in (2b) by numerically evaluating the near-field surface integrations given by [15, eqs. 107–111, Ch. 6], solving (2b) for $\overline{I}_{\mathrm{obj}}^{(1)}$, updating $\overline{V}_g^{(1)}$ in (2a), and finally solving (2a) for $\overline{I}_g^{(1)}$. These steps represent one interaction mechanism (i.e., ground–object–ground) that should be repeated until convergence of surface current solutions is achieved. The final updated electric and magnetic surface currents on the ground will be $\overline{J}_g = \overline{J}_g^{(0)} + \overline{J}_g^{(1)} +$

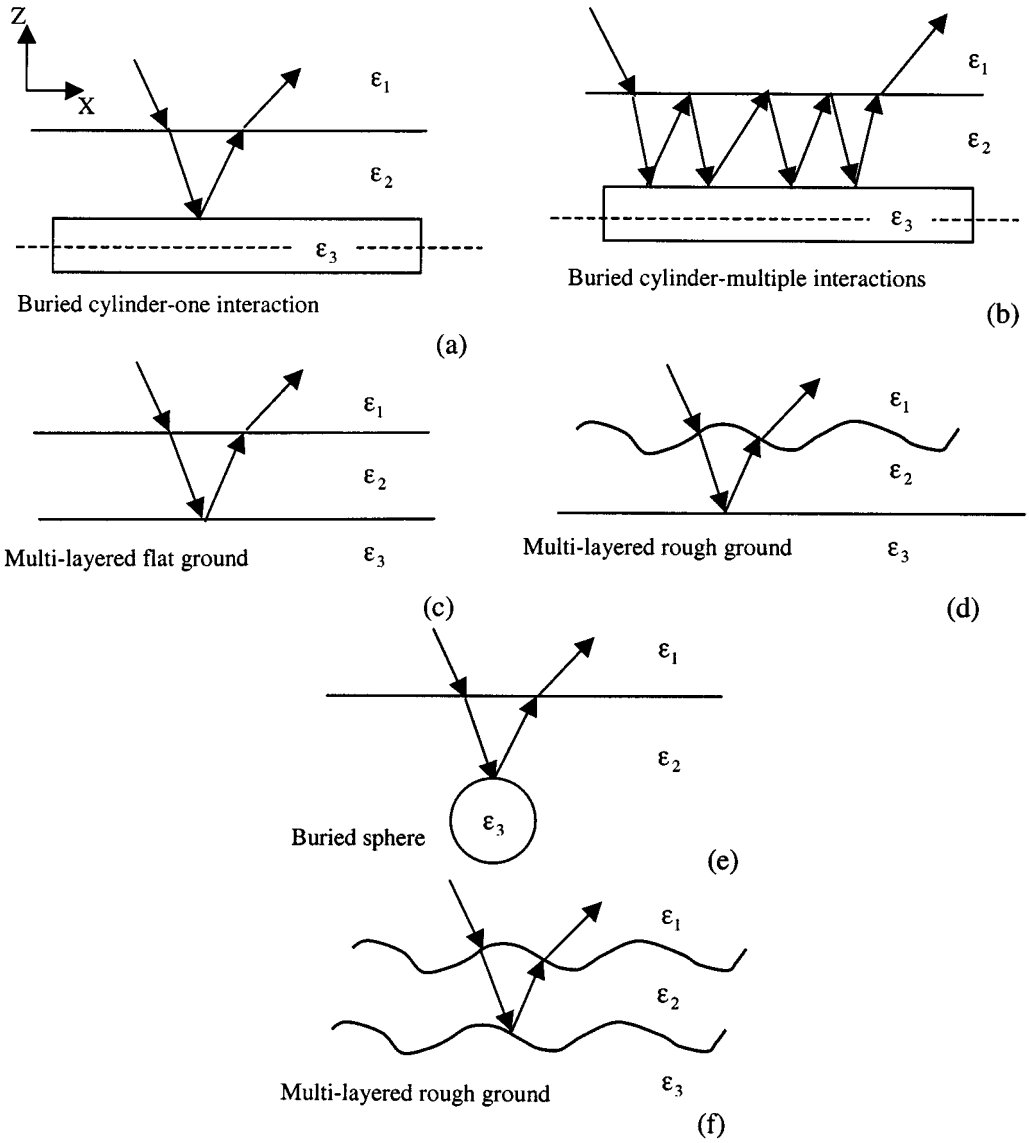

Fig. 2. (a) A cylinder of length $b = 3.04\lambda_0$, radius $a = 0.15\lambda_0$ and $\varepsilon_{3r} = 7.9 - j0.0029$ buried at $z = -0.65\lambda_0$ under a flat ground of dimensions $3.04\lambda_0 \times 3.04\lambda_0$ with $\varepsilon_{2r} = 2.5 - j0.18$ for $\vartheta^i = 0^\circ$ (Example 1), showing one ground–object–ground mechanism $n = 1$. (b) The same data of (a) showing four ground–object–ground mechanisms $n = 4$. (c) The same flat air–ground interface of (a) and a flat under ground layer buried at $z = -0.45\lambda_0$ with $\varepsilon_{3r} = 4.2 - j0.29$ for $\vartheta^i = 10^\circ$ (Example 2). (d) The same data of (c) but with rough air/ground interface with rms height $\sigma = 0.08\lambda_0$ and correlation length $l_c = 0.5\lambda_0$ (Example 3). (e) A sphere of radius of $a = 0.5\lambda_0$ with $\varepsilon_{3r} = 4.5 - j0.029$ buried at $z = -0.75\lambda_0$ (measured from its center) under a flat air/ground interface of dimensions $4.08\lambda_0 \times 4.08\lambda_0$ with $\varepsilon_{2r} = 2.5 - j0.18$ for $\vartheta^i = 0^\circ$ (Example 4). (f) The same data of (e) but with rough air/ground ($\sigma_1 = 0.06\lambda_0$, $l_{c1} = 0.5\lambda_0$) and underground interface ($\sigma_2 = 0.05\lambda_0$, $l_{c2} = 0.4\lambda_0$) buried at $z = -0.95\lambda_0$ (measured between the two mean planes) with $\varepsilon_{3r} = 3.7 - j0.2$ (Example 5).

$\overline{J}_g^{(2)} + \cdots + \overline{J}_g^{(n)}$ and $\overline{M}_g = \overline{M}_g^{(0)} + \overline{M}_g^{(1)} + \overline{M}_g^{(2)} + \cdots + \overline{M}_g^{(n)}$, respectively, and on the object $\overline{J}_{\rm obj} = \overline{J}_{obj}^{(1)} + \overline{J}_{obj}^{(2)} + \overline{J}_{\rm obj}^{(3)} + \cdots + \overline{J}_{\rm obj}^{(n)}$ and $\overline{M}_{\rm obj} = \overline{M}_{obj}^{(1)} + \overline{M}_{\rm obj}^{(1)} + \overline{M}_{obj}^{(2)} + \cdots + \overline{M}_{\rm obj}^{(n)}$, respectively. In order to accelerate the computations, the SDFMM can be used separately in (2a) and in (2b) to convert each dense impedance matrix $\overline{Z}_{g.g}$ and $\overline{Z}_{\rm obj.obj}$ into a sparse one leading to the multiple interaction model with the SDFMM. However, the efficient use of the SDFMM is contingent on the geometry of each scatterer separately, i.e., both the rough ground and the buried object should be quasiplanar structures. In this case, one interaction mechanism between the ground and the buried scatterer requires solving (2a) two times, solving (2b) only once, and numerically evaluating the near field expressions in [15] once for the object's and once for the ground's incident fields. This implies that SDFMM is not used in the near-field interaction computations given in [15]. Thus, if K_1 and K_2 are the number of the RWG triangular patches on the rough ground and on the object, respectively, then evaluating the near-field expressions in [15] using patch–patch interactions requires $2K_1K_2$ operations [16]. Moreover, all the information needed to evaluate these surface integrations are pre-calculated and prestored during the computations of $\overline{Z}_{g.g}$ and $\overline{Z}_{obj.obj}$. Thus, the overall number of operations for the multiple interaction model with the SDFMM is proportional to $2N + 2N + 2P + 4K_1K_2 = (4N + 2P + 4K_1K_2)$. The quantity $(4K_1K_2)$ can be approximated by $(16NP/9 \approx 2NP)$ [16]. However, it is crucial to indicate that these $(2NP)$ operations are conducted only once in each interaction mechanism and they are not conducted in every iteration of the iterative solver like the $(4N + 2P)$ operations. The Transpose Free Quasi Minimal Residual (TFQMR) iterative solver is used in this work [17]. The memory requirements in the multiple interaction model with the SDFMM is $O(2N + 2P)$. On the other hand, the computational complexity of the complete SDFMM is $O(2N+2P)$ [3], [7], [8], the conventional MoM is of $O((2N+2P)^2)$, and the multiple interaction model is of $O(4N^2 + 4P^2)$ for both the

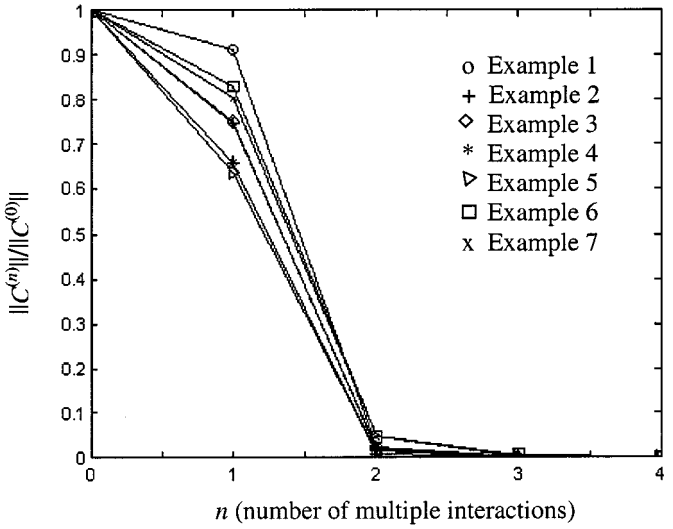

Fig. 3. The normalized change in the surface currents $\|C^{(n)}\|/\|C^{(0)}\|$ versus the number of interactions for Examples 1–7, where the vector C contains all electric and magnetic surface currents.

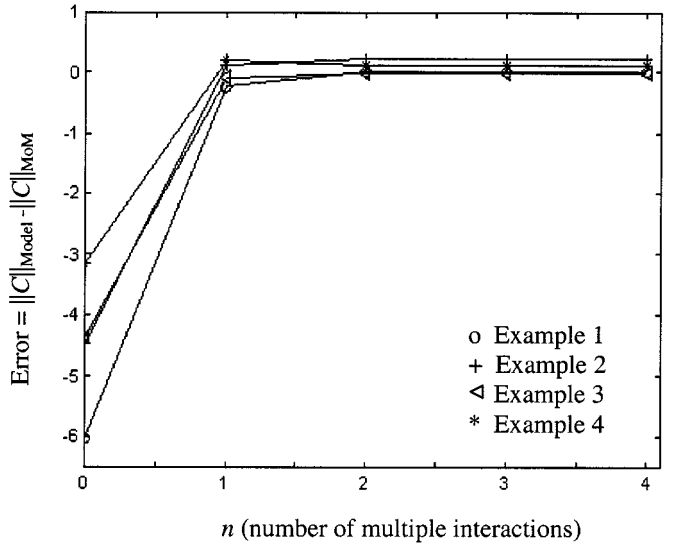

Fig. 4. The error in the norm of the surface currents obtained using the multiple interaction model $\|C\|_{\text{Model}}$ and those obtained using the conventional MoM ($\|C\|_{\text{MoM}}$) versus the number of interactions for Examples 1–4, where the vector C contains all electric and magnetic surface currents.

CPU time and computer memory. In the case where the buried scatterer has a nonquasi-planar structure but instead has a small electrical size, the multiple interaction model can still be used by solving (2a) using the SDFMM while solving (2b) using the MoM (i.e., the multiple interaction model with partial use of the SDFMM). This scenario will slightly increase the total computational operations. However, if the nonquasi-planar buried scatterer has a very large electrical size, then using the MoM to solve (2b) will lead to a significant increase in the computational operations. In addition, the coupling $(2NP)$ operations per interaction will increase as well which limits the use of the multiple interaction model for this case.

III. Numerical Results

Basically we are interested in subsurface sensing problems where calculating the surface currents on the rough ground dominates the overall computations. In all results presented in this section, the incident wave is assumed to be a Gaussian beam tapered toward the edges of the ground [18] with horizontally polarized incident electric field (i.e., in the y direction). The half-beam width is $L/5$ where the ground has dimensions $L \times L$.

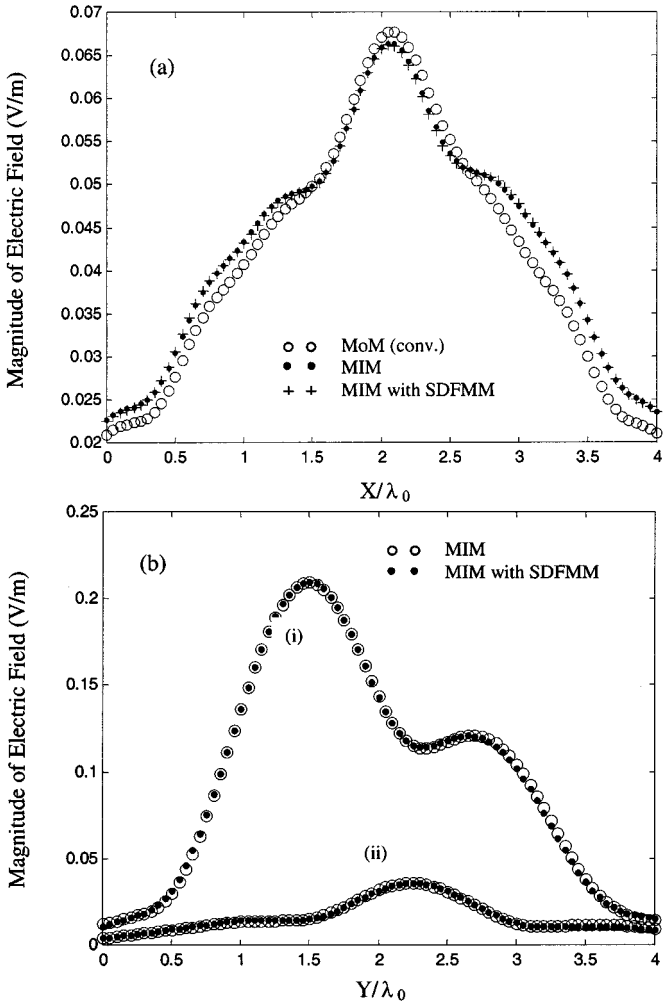

Fig. 5. Magnitude of scattered electric field $|\overline{E}|$ received at $z = 0.5\lambda_0$ above the ground due to (a) just the buried sphere in Example 4 [Fig. 2(e) shown at $y = 2.04\lambda_0$] and (b) due to 1) just the rough air/ground interface and 2) just the rough underground layer, in Example 5 [Fig. 2(f) shown at $x = 2.04\lambda_0$].

A variety of geometries represented by seven examples are used in this section. For Examples 1–5, the geometries are described in Fig. 2(a)–(f) where the ground media is lossy with relative dielectric constant assumed as $\varepsilon_{2r} = 2.5 - j0.18$. However, to investigate the case of a shallow scatterer buried in a lossless medium, Example 6 uses the geometry in Fig. 2(c) but for larger dimensions of the ground given by $4.08\lambda_0 \times 4.08\lambda_0$ with $\varepsilon_{2r} = 2.5$ while the underground layer is assumed to have $\varepsilon_{3r} = 6.7 - j0.2$ and is buried at $z = -0.1\lambda_0$. The same geometry is also used in Example 7, but with even larger dimensions of the ground given by $8\lambda_0 \times 8\lambda_0$, same lossless soil of $\varepsilon_{2r} = 2.5$, and lossy underground layer of $\varepsilon_{3r} = 6.7 - j1.0$ buried at $z = -0.1\lambda_0$. The accuracy of the near-field expressions in [15] deteriorates for burial depths smaller than $0.1\lambda_0$ since the source and observation points become very close to each other.

A qualitative comparison (not presented here) showed excellent agreement between the surface currents obtained using the multiple interaction model with those obtained using the conventional MoM. Moreover, the convergence of the surface current solutions

TABLE I
CPU TIME AND COMPUTER MEMORY REQUIREMENTS FOR EXAMPLES 1–5

Examples	# Unknowns		# Patches		CPU (min.)			Memory (MB)		
	$2N$	$2P$	K_1	K_2	MoM (conv.)	MIM	MIM with SDFMM	MoM (conv.)	MIM	MIM with SDFMM
1 (Fig. 2a)	8512	8352	2888	2808	118	49	†	1280	850	†
2 (Fig. 2c)	8512	8512	2888	2888	72	37	†	1305	880	†
3 (Fig. 2d)	8512	8512	2888	2888	78	38	†	1305	880	†
4 (Fig. 2e)	15402	2292	5202	764	93	66	38	1848	1467	225
5 (Fig. 2f)	15402	15402	5202	5202	‡	130	45	>6000	3256	395
7 (Fig. 2c)	59600	59600	20000	20000	‡	‡	192	‡	‡	1818

† The emphasis is to validate the MIM with the MoM for these small cases.
‡ The MoM could not be used for this case due to the large memory requirements (> 6 GB).

in Examples 1–7, is quantitatively demonstrated by plotting the normalized change in the currents $\|C^{(n)}\|/\|C^{(0)}\|$ versus the number of interactions between the ground and the buried scatterer. This is shown in Fig. 3. The vector C has dimensions of $(2N + 2P)$ and it contains all the electric and magnetic surface currents on both the air/ground interface and the buried scatterer. The results show that a significant change occurs in the currents after one interaction ($n = 1$); however, much less significant change in the currents is observed after two interactions ($n = 2$), as shown for Examples 6 and 7, where the maximum relative change in the currents is less than 5%. However, insignificant changes are observed for all cases at the third or higher interaction. This indicates that the contributions from the higher interactions depend on the physical properties of the scatterer, and in some cases, larger changes in the currents may occur at the second interaction. In Fig. 4, the error in the norm of the surface currents obtained using the multiple interaction model $\|C\|_{\rm Model}$ and those obtained using the conventional MoM ($\|C\|_{\rm MoM}$) are plotted versus the number of interactions for Examples 1–4. The results clearly validate the multiple interaction model.

In Fig. 5(a), the scattered electric fields received above the ground at $z = 0.5\lambda_0$ and due just to the buried sphere are plotted versus the x-direction for $y = 2.04\lambda_0$ using the data of Example 4 [Fig. 2(e)]. Three solutions are obtained for this example: 1) the conventional MoM for the whole scatterer; 2) the multiple interaction model (MIM); and 3) the multiple interaction model with the SDFMM (MIM with SDFMM). The observed slight differences are attributed to the difference in defining the scattered fields due to just the buried sphere in both the conventional MoM and the multiple interaction model. Using the conventional MoM, we calculated the total scattered electric fields twice; with and without the buried sphere, then the results are subtracted from each other with complex vectors [7], [8]. On the other hand, using the multiple interaction model, we use the obtained surface currents on the ground due to only the presence of the sphere, i.e., $\overline{J}_g^{(1)} + \overline{J}_g^{(2)} + \overline{J}_g^{(3)}$ and $\overline{M}_g^{(1)} + \overline{M}_g^{(2)} + \overline{M}_g^{(3)}$, and incorporate them into the near-field expressions in [15] to compute the scattered electric fields above the ground. Notice that the quantities $\overline{J}_g^{(0)}$ and $\overline{M}_g^{(0)}$, the surface currents on the ground without a buried object, are not used in the calculations of the object signature. In Fig. 5(b), the scattered electric fields received above the ground at $z = 0.5\lambda_0$ are plotted versus the y-direction for $x = 2.04\lambda_0$ using the data of Example 5 [Fig. 2(f)]. The scattered fields due to just the air–ground rough interface are calculated using only the ground surface currents without the presence of the buried layer, i.e., $\overline{J}_g^{(0)}$ and $\overline{M}_g^{(0)}$, while the scattered fields due to just the underground rough layer are calculated using only the ground surface currents $\overline{J}_g^{(1)} + \overline{J}_g^{(2)} + \overline{J}_g^{(3)}$ and $\overline{M}_g^{(1)} + \overline{M}_g^{(2)} + \overline{M}_g^{(3)}$. As expected, the signature of the air–ground rough interface is significantly larger than that of the underground rough layer. Table I summarizes all examples considered in this section obtained using the conventional MoM, the MIM, and the MIM with the SDFMM. All these three models are calculating the surface currents on the air/ground interface and on the buried object. The overall computer memory and CPU time are given for one interaction mechanism (i.e., ground–object–ground). In Example 7, the total CPU time is 192 min—177 min for the TFQMR iterative solver and only 15 min for updating the incident fields on both the ground and the underground layer (interactions). This represents less than 8% of the total CPU time.

In all results presented in this section, a relative residual error of 10^{-5} is used in the TFQMR iterative solver [17] and the smallest FMM block size is assumed to be $0.32\lambda_0 \times 0.32\lambda_0$. In Examples 1–4, upon comparing the use of the MIM with the conventional MoM, the reductions in the total CPU time and computer memory, range from 30% to 60% and from 20% to 35%, respectively. On the other hand, the CPU time and computer memory are reduced by almost 65% and 88%, respectively, when the MIM with the SDFMM is used versus the MIM as shown in Example 5. Moreover, in Example 7, only the MIM with the SDFMM could be used due to the huge required computer memory (>6 GB) for both the MoM and the MIM.

It is necessary to emphasize that the most attractive feature of the MIM with the SDFMM is removing the quasi-planar structure constraint to enable its use in the nonquasi-planar applications described in Fig. 2. Moreover, there are no overlapping applications that require choosing between the MIM with the SDFMM, which works more efficiently for nonshallow scatterers, and the complete SDFMM in [7], [8], which works more efficiently for shallow scatterers. However, to obtain the signature of the buried scatterer, the complete SDFMM in [7] and [8] requires executing the computer code twice, with and without the buried object, while the MIM with the SDFMM computes the object signature by running the computer code only once. Even thought no convergence problems were encountered in any of the tested cases, even when a very shallow underground layer is buried in lossless soil; however, for shallow scatterers, the complete SDFMM in [7] and [8] should be used since it represents a potentially nonstationary algorithm for the whole matrix as discussed in [19] in addition to its superior computational complexity when used for the whole scatterer.

IV. CONCLUSION

The multiple interaction approach is used with the robust SDFMM to remove the quasi-planar structure constraint to enable analyzing nonshallow objects buried beneath the 2-D random rough ground. The results show that the first interaction mechanism between the ground and the buried scatterer significantly contributes to the surface current solutions while the contributions of additional interactions become insignificant, especially when the nonshallow object is buried in lossy background soil.

ACKNOWLEDGMENT

The SDFMM algorithm was originally developed at the University of Illinois of Urbana-Champaign by V. Jandhyala, E. Michielssen, and W. Chew.

REFERENCES

[1] V. Rokhlin, "Rapid solution of integral equations of scattering theory in two dimensions," *J. Comput. Phys.*, vol. 36, pp. 414–439, 1990.

[2] C. C. Lu and W. C. Chew, "A multilevel fast-algorithm for solving a boundary integral equation of wave scattering," *Microwave Opt. Tech. Let.*, vol. 7, pp. 466–470, July 1994.

[3] V. Jandhyala, "Fast multilevel algorithms for the efficient electromagnetic analysis of quasiplanar structures," Ph.D. dissertation, Dept. Elect. Comput. Eng., Univ. Illinois, Urbana-Champaign, 1998.

[4] S. Li, C. H. Chan, L. Tsang, Q. Li, and L. Zhou, "Parallel implementation of the sparse matrix/canonical grid method for the analysis of two-dimensional random rough surfaces (three-dimensional scattering problem) on a Beowulf system," *IEEE Trans. Geosci. Remote Sensing*, vol. 38, pp. 1600–1608, July 2000.

[5] D. Torrungrueng, H. Chou, and J. T. Johnson, "A novel acceleration algorithm for the computation of scattering from two-dimensional large scale perfectly conducting random rough surfaces with the forward–backward method," *IEEE Trans. Geosci. Remote Sensing*, vol. 38, pp. 1656–1666, July 2000.

[6] N. Geng, A. Sullivan, and L. Carin, "Multilevel fast-multipole algorithm for scattering from conducting targets above or embedded in a lossy half space," *IEEE Trans. Geosci. Remote Sensing*, vol. 38, pp. 1561–1573, July 2000.

[7] M. El-Shenawee, C. Rappaport, E. Miller, and M. Silevitch, "3-D subsurface analysis of electromagnetic scattering from penetrable/PEC objects buried under rough surfaces: Use of the steepest descent fast multipole method (SDFMM)," *IEEE Trans. Geosci. Remote Sensing*, vol. 39, pp. 1174–1182, June 2001.

[8] M. El-Shenawee, C. Rappaport, and M. Silevitch, "Monte Carlo simulations of electromagnetic wave scattering from random rough surface with 3-D penetrable buried object: Mine detection application using the SDFMM," *J. Opt. Soc. Amer. A*, vol. 18, pp. 3077–3084, Dec. 2001.

[9] E. Bahar and M. El-Shenawee, "Full wave single and multiple scattering from rough surfaces," *J. Comput. Phys.*, vol. 115, pp. 390–398, Dec. 1994.

[10] E. Bahar and Y. Zhang, "Diffuse like and cross-polarized fields scattered from irregular layered structures-full wave analysis," *IEEE Trans. Antennas Propagat.*, vol. 47, pp. 941–948, May 1999.

[11] G. Zhang, L. Tsang, and K. Pak, "Angular correlation function and scattering coefficient of electromagnetic waves scattered by a buried object under a two-dimensional rough surface," *J. Opt. Soc. Amer. A*, vol. 15, no. 12, pp. 2995–3002, Dec. 1998.

[12] J. T. Johnson, "A study of the four-path model for scattering from an object above a halfspace," *Microwave Opt. Tech. Lett.*, vol. 30, pp. 130–134, July 2001.

[13] J. T. Johnson and R. J. Burkholder, "Coupled canonical grid/discrete dipole approach for computing scattering from objects above or below a rough interface," *IEEE Trans. Geosci. Remote Sensing*, vol. 39, pp. 1214–1220, June 2001.

[14] L. Li, Jiangqi, Z. Liu, and L. Carin, "MLFMA analysis of scattering from multiple targets in the presence of a half space," *IEEE Trans. Antennas Propagat.*, to be published.

[15] C. A. Balanis, *Advanced Engineering Electromagnetics.* New York: Wiley, 1989, ch. 6, pp. 254–309.

[16] S. M. Rao, D. R. Wilton, and A. W. Glisson, "Electromagnetic scattering by surfaces of arbitrary shape," *IEEE Trans. Antennas Propagat.*, vol. AP-30, pp. 409–418, May 1982.

[17] R. W. Freund, "A transpose-free quasiminimal residual algorithm for nonhermitian linear systems," *SIAM J. Sci. Comput.*, vol. 14, no. 2, pp. 470–482, Mar. 1993.

[18] P. Tran and A. A. Maradudin, "Scattering of a scalar beam from a two-dimensional randomly rough hard wall: Enhanced backscatter," *Phy. Rev. B*, vol. 45, no. 7, pp. 3936–3939, Feb. 1992.

[19] J. C. West and J. M. Sturm, "On iterative approaches for electromagnetic rough-surface scattering problems," *IEEE Trans. Antennas Propagat.*, vol. 47, pp. 1281–1288, Aug. 1999.